J. Space Weather Space Clim. 2018, 8, A54

https://doi.org/10.1051/swsc/2018043

JSWSC

Available online at:
www.swsc-journal.org

Planetary Space Weather

RESEARCH ARTICLE OPEN ACCESS

# Shock deceleration in interplanetary coronal mass ejections (ICMEs) beyond Mercury's orbit until one AU

Benjamin Grison[1,*], Jan Souček[1], Vratislav Krupar[2,3,1], David Píša[1], Ondrej Santolík[1,4], Ulrich Taubenschuss[1], and František Němec[4]

[1] Department of Space Physics, Institute of Atmospheric Physics, Czech Academy of Sciences, Boční II 1401, 141 31 Prague 4, Czech Republic
[2] Universities Space Research Association, 21046 Columbia, MD, USA
[3] NASA Goddard Space Flight Center, 20771 Greenbelt, MD, USA
[4] Faculty of Mathematics and Physics, Charles University, 180 00 Prague 8, Czech Republic

Received 27 April 2018 / Accepted 31 October 2018

**Abstract –** The CDPP propagation tool is used to propagate interplanetary coronal mass ejections (ICMEs) observed at Mercury by MESSENGER to various targets in the inner solar system (VEX, ACE, STEREO-A and B). The deceleration of ICME shock fronts between the orbit of Mercury and 1 AU is studied on the basis of a large dataset. We focus on the interplanetary medium far from the solor corona, to avoid the region where ICME propagation modifications in velocity and direction are the most drastic. Starting with a catalog of 61 ICMEs recorded by MESSENGER, the propagation tool predicts 36 ICME impacts with targets. ICME in situ signatures are investigated close to predicted encounter times based on velocities estimated at MESSENGER and on the default propagation tool velocity (500 km $s^{-1}$). ICMEs are observed at the targets in 26 cases and interplanetary shocks (not followed by magnetic ejecta) in two cases. Comparing transit velocities between the Sun and MESSENGER ($\overline{v}_{SunMess}$) and between MESSENGER and the targets ($\overline{v}_{MessTar}$), we find an average deceleration of 170 km $s^{-1}$ (28 cases). Comparing $\overline{v}_{MessTar}$ to the velocities at the targets ($v_{Tar}$), average ICME deceleration is about 160 km $s^{-1}$ (13 cases). Our results show that the ICME shock deceleration is significant beyond Mercury's orbit. ICME shock arrival times are predicted with an average accuracy of about six hours with a standard deviation of eleven hours. Focusing on two ICMEs detected first at MESSENGER and later on by two targets illustrates our results and the variability in ICME propagations. The shock velocity of an ICME observed at MESSENGER, then at VEX and finally at STEREO-B decreases all the way. Predicting arrivals of potentially effective ICMEs is an important space weather issue. The CDPP propagation tool, in association with in situ measurements between the Sun and the Earth, can permit to update alert status of such arrivals.

**Keywords:** Interplanetary Coronal Mass Ejection (CME) / interplanetary medium / propagation / space weather / multipoint analysis

## 1 Introduction

Solar coronal mass ejections (CMEs) can trigger intense space weather events (Gonzalez et al., 2007). In order to predict potential consequences, it is important to understand the propagation of interplanetary CMEs (ICMEs) and magnetic clouds (MCs), which are a subset of ICMEs, in the interplanetary medium. An ICME magnetic ejecta is often preceded by an interplanetary shock (ICME shock) and a sheath.

The temporal delay between an eruption of a CME at the Sun and its impact at Earth, i.e. the maximum of geomagnetic activity, was found to be in many cases 80 h, which corresponds to a mean ICME propagation velocity of 500 km $s^{-1}$ (Brueckner et al., 1998). Assuming that slow CMEs are accelerated by the surrounding interplanetary medium and that fast CMEs are decelerated can explain the observed travel times. Gopalswamy et al. (2000, 2001a) found evidence of such acceleration/deceleration by comparing CME velocities (coronagraph observations) to ICME velocities (in situ observations).

The NASA STEREO mission (Kaiser et al., 2008) improved our understanding of the ICME velocity evolution in the interplanetary medium by means of stereoscopic images (Davis et al., 2009). The ICME speed along its Sun-to-Earth

*Corresponding author: grison@ufa.cas.cz

journey can be monitored with a triangulation technique based on STEREO observations (Liu et al., 2010). Based on a few case studies, CME acceleration seems to be confined to distances of 10 solar radii ($R_\odot$), and fast CMEs become decelerated between mainly 20 and 50 $R_\odot$ distance (Liu et al., 2016; Manchester et al., 2017).

This makes CME/ICME association complex (Bocchialini et al., 2018) and wrong associations lead to wrong transit velocity estimations. CME channelling (Möstl et al., 2015) and CME-CME interaction (Gopalswamy et al., 2001b), identified by radio type II burst intense continuum-like emission, make the CME/ICME association more tricky. In situ measurements farther from the solar corona permit to study the ICME shock deceleration in the interplanetary medium, avoiding the region where a drastic change can be observed in ICME propagation.

Following ICMEs between different vantage points in the solar system has been done up to Saturn (Prise et al., 2015) or Pluto (Witasse et al., 2017). Alternative to magnetic structures authors frequently use the Forbush decrease to identify ICMEs at various targets (Möstl et al., 2015; Freiherr von Forstner et al., 2018; Winslow et al., 2018). Witasse et al. (2017) studied an ICME that progressively slowed down from the Sun to Earth, Mars, Comet 67P, and possibly Pluto. Prise et al. (2015) noted unexpected ICME acceleration after an interaction with high-speed jets. Considering 15 events Freiherr von Forstner et al. (2018) noted ICME deceleration between the solar corona and L1 (170 km $s^{-1}$) and between Earth and Mars (67 km $s^{-1}$, based on Forbush decrease observations).

Radial propagation of ICMEs or of ICME shocks in the solar system can be studied with the *Centre de Données de Physique des Plasmas* (CDPP) Propagation Tool (Rouillard et al., 2017) which is publicly available at http://propagationtool.cdpp.eu/. Witasse et al. (2017) successfully followed ICME propagation from the Sun to Pluto with this tool. We propose here to test the ability of the Propagation Tool by tracking ICMEs between MESSENGER and different probes up to 1 AU. All ICMEs are part of a catalog which is based on NASA MESSENGER observations (Winslow et al., 2015). The aim of this study is to estimate the ICME shock acceleration/deceleration between Mercury's orbit and the orbit of Venus (VEX observations) as well as out to a distance of 1 AU (ACE and STEREO observations). We also want to test the utility of the tool to reduce the number of false alerts of potential effective ICMEs when in situ measurements are available in real-time between the Sun and the Earth.

Our dataset and methodology are detailed in Section 2. The ICME hits of VEX, ACE and STEREO probes predicted by the Propagation Tool are compared to in situ observations in Section 3. We comment on the ICME acceleration beyond Mercury's orbit up to 1 AU in Section 4. Before concluding we put special attention to ICMEs observed by two spacecraft beyond Mercury's orbit (Sect. 5).

## 2 Data set and terminology

We based our study on a catalog of ICME observations by the NASA spacecraft MESSENGER at Mercury, which lasts from 19 May 2011 until 2 September 2014 (Winslow et al., 2015). Running the Propagation Tool in radial propagation mode for each of the 61 events in the catalog, we identify the ICMEs that probably hit another object besides MESSENGER up to one AU. These objects, or targets, are VEX that orbits around Venus, ACE, and STEREO-A and B spacecraft orbiting at ≈1 AU. In addition to the starting point, MESSENGER in the present case, the necessary inputs for the radial propagation option are: ICME radial velocity (default value $v_{def}$ = 500 km $s^{-1}$), the angular size of the CME at the Sun (default value $\alpha_{CME} = 45^\circ$) and the choice of the target. There is no measurement of the plasma bulk flow velocity available at MESSENGER, so we do not consider the drag option available in the Propagation Tool. That option permits to brake or speed up ICME velocity depending on the preceding solar wind velocity. The ICME shock acceleration (positive or negative) is studied by looking for an input radial velocity that matches with observation times at MESSENGER ($t_{obsMESS}$) and the targets ($t_{obsTAR}$). We then compare this velocity ($\overline{v}_{MessTar}$) to the velocity at MESSENGER ($\overline{v}_{SunMess}$) and at the targets ($v_{Tar}$).

**Table 1.** Classification of the 36 pairs predicted by the Propagation Tool. ICME, IP, Void and No data tags are explained in the text. ICMEs that interacted with another ICME between MESSENGER and the targets are counted separately (+). Note that there is no False prediction (see comments in the text).

| Target | Pairs | False | Correct | | Discarded | |
|---|---|---|---|---|---|---|
| | | | ICME | IP | Void | No data |
| VEX | 15 | 0 | 10 + 1 | 0 | 3 | 1 |
| ACE | 4 | 0 | 4 | 0 | 0 | 0 |
| STEREO-A | 11 | 0 | 8 + 2 | 0 | 0 | 1 |
| STEREO-B | 6 | 0 | 4 | 2 | 0 | 0 |
| Total | 36 | 0 | 26 + 3 | 2 | 3 | 2 |

When the Propagation Tool predicts a target hit by an ICME we refer to the MESSENGER observations and the target observations as a pair. For every pair, we check the data observed at the target around the predicted impact times ($t_{predV500}$ and $t_{predVmes}$) for signatures of an ICME, considering all the datasets which are publicly available on the AMDA web tool (http://amda.cdpp.eu/).

ICMEs have distinct plasma and magnetic field properties which differentiate them from the surrounding solar wind. An ideal magnetic signature of a magnetic cloud (MC) is a force-free field, which corresponds to a steady rotation of the magnetic field vector as the MC is sweeping over the observer (Burlaga et al., 1981). ICME identification also relies on additional parameters such as a low plasma density, a low plasma temperature, high abundances of heavy elements, or typical signatures of energetic particles compared to typical solar wind conditions (e.g., Gosling et al., 1973; Cane & Richardson, 2003; Liu et al., 2005; Malandraki et al., 2005, 2007, and references therein). Typically, ICMEs match only some of these criteria (Richardson & Cane, 1993).

Cane & Richardson (2003) noticed that magnetic rotation in ICMEs often does not agree with a force-free field, and hence

> "a likely ICME interval can be inferred from reduced fluctuations and some degree of organization in the magnetic field and is bounded by distinct magnetic field discontinuities which may be accompanied by abrupt changes in plasma parameters".

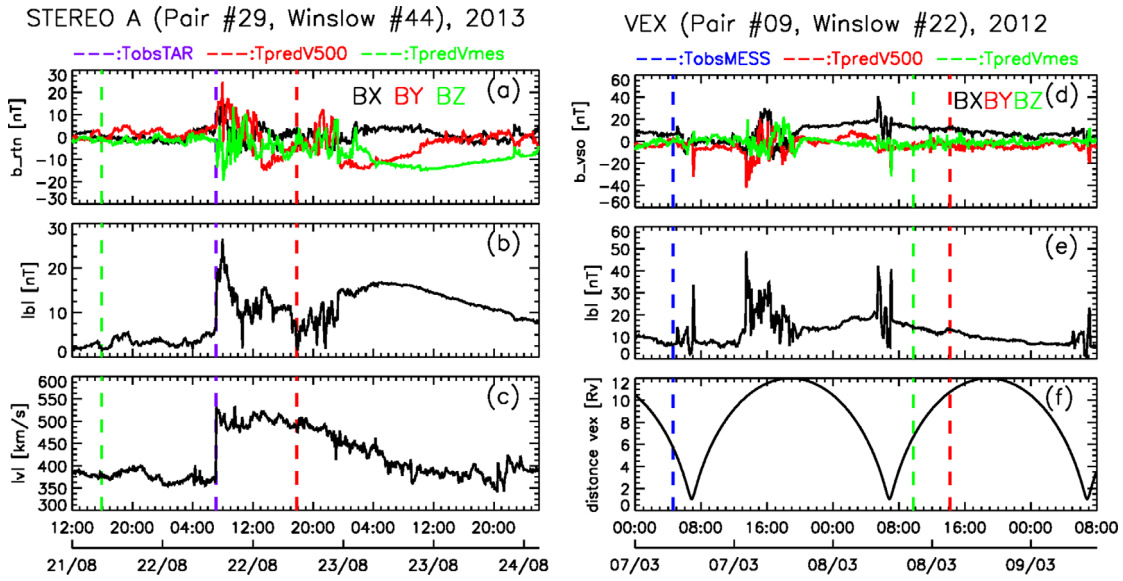


**Fig. 1.** Example of events categorized as Correct (left, STEREO-A data) and as Void (right, VEX data). Top panels: three components of the magnetic field (***B***); central panels: ***B*** intensity; bottom panels: bulk flow velocity (left) and Venus-VEX distance (right). Vertical dashed lines indicate shock observation times at STEREO-A (violet) and at MESSENGER (blue) and shock arrival predicted times (red and green colors).

Winslow et al. (2015) identified ICMEs from magnetic field observations only. They select events with a clear interplanetary shock at the time of arrival, followed by a sheath and a magnetic ejecta region. Assuming that an ICME's magnetic configuration is preserved during its propagation, we proceed in the same way at the target by looking for periods exhibiting a structured interplanetary magnetic field (IMF), preferably including a smooth rotation, and a preceding shock and sheath. When possible, this ICME identification is confirmed with in situ solar wind observations. For each pair, observations at the target are classified as No Data, Void, ICME and IP (cf. Table 1): No Data when no magnetic data are available; Void (VEX only) when ICME shock arrival could be hidden to VEX due to its proximity to Venus (see right panel of Fig. 1 and related text for more explanations); ICME when observing a magnetic ejecta and additional convincing plasma parameters (density, velocity, $\alpha$-particle to proton ratio, temperature, as previously defined) are present; and IP when the observed interplanetary shock is not followed by any magnetic ejecta. We compared our results with the following ICME catalogs: HELCATS (https://www.helcats-fp7.eu/catalogues/wp4_icmecat.html), STEREO (Jian et al., 2018) and ACE (http://www.srl.caltech.edu/ACE/ASC/DATA/level3/icmetable2.htm; described in Richardson & Cane, 2010). We finally check for each pair ICME propagation between Mercury and the target in ENLIL simulations (Odstrcil & Pizzo, 1999, 2009) available online (http://helioweather.net/index.html).

We distinguish among the following times and velocities:

- $t_{\mathrm{obsMESS}}$: ICME shock arrival time observed at MESSENGER (Winslow et al., 2015). $t_{\mathrm{obsMESS}}$ is defined for all the records.
- $t_{\mathrm{obsTAR}}$: ICME shock arrival time observed at the target. It is defined for ICME and IP events.
- $\overline{v}_{\mathrm{SunMess}}$: shock transit speed at MESSENGER (Winslow et al., 2015). $\overline{v}_{\mathrm{SunMess}}$ is derived from the time delay between the CME onset at the Sun and its arrival at MESSENGER. We want to emphasize that $\overline{v}_{\mathrm{SunMess}}$ is not the measured velocity at MESSENGER but rather an average velocity of the shock between the solar corona and MESSENGER. It relies on a CME/ICME association. Winslow et al. (2015) do not specify how they select the solar source. $\overline{v}_{\mathrm{SunMess}}$ is defined for all the pairs.
- $\overline{v}_{\mathrm{MessTar}}$: this is a constant ICME velocity which is set in the Propagation Tool. $\overline{v}_{\mathrm{MessTar}}$ fits with both ICME shock arrival times at MESSENGER $t_{\mathrm{obsMESS}}$ and at the targets $t_{\mathrm{obsTAR}}$. $\overline{v}_{\mathrm{MessTar}}$ is defined for ICME and IP events. $\overline{v}_{\mathrm{MessTar}}$ is the average velocity of the shock between MESSENGER and the target.
- $v_{\mathrm{Tar}}$: observed ICME shock velocity by the target spacecraft. $v_{\mathrm{Tar}}$ is defined for ICME and IP events, when solar wind velocity measurements are available at the target.
- $t_{\mathrm{predV500}}$: ICME shock arrival time at the target predicted by the tool based on a default propagation velocity of 500 km $\mathrm{s}^{-1}$ between MESSENGER and the target. It is defined for all the pairs.
- $t_{\mathrm{predVmes}}$: ICME shock arrival time at the target predicted by the tool based on $\overline{v}_{\mathrm{SunMess}}$. $t_{\mathrm{predVmes}}$ is defined for all the records.

We focus on the ICME shock propagation rather than on the magnetic ejecta itself because the shock timing appears to be more precise and somehow less subjective than the timing of the boundaries of the magnetic ejecta.

## 3 Analysis of the predicted hits

Running the tool on the 61 catalog records, 36 pairs are found as detailed in Table 1. There are no magnetic field measurements at target for STEREO-A and VEX No Data events. VEX is close to its periapsis around the predicted hit times in the three Void events. One of these events is described

**Table 2.** Details of the 36 pairs. A number is assigned to each pair. Pairs are sorted first by target names and then in chronological order. id refers to the event number in the list of Winslow et al. (2015). $t_{obsMESS}$, $t_{obsTAR}$, $\overline{v}_{SunMess}$, $\overline{v}_{MessTar}$, and $v_{Tar}$ are defined in Section 2. $\Delta t_{V500} = t_{obsTAR} - t_{predV500}$ and $\Delta t_{Vmess} = t_{obsTAR} - t_{predVmes}$. Note that $\Delta t_{V500}$ and $\Delta t_{Vmess}$ are time differences between observations and predictions.

| Pair | Target | Id | $t_{obsMESS}$ | $t_{obsTAR}$ | Cat. | $\Delta t_{Vmess}$ hh:mm | $\Delta t_{V500}$ hh:mm | $\overline{v}_{SunMess}$ km s$^{-1}$ | $\overline{v}_{MessTar}$ km s$^{-1}$ | $v_{Tar}$ km s$^{-1}$ |
|---|---|---|---|---|---|---|---|---|---|---|
| #01 | VEX | W02 | 2011-Jun-04 15:12 | Jun-05 05:25 | ICME | 03:31 | −18:59 | 1552 | 1165 | |
| #02 | VEX | W03 | 2011-Jun-05 03:31 | Jun-05 12:10 | ICME† | 01:34 | −24:44 | 2359 | 1920 | |
| #03 | VEX | W04 | 2011-Jun-11 04:25 | VOID | | | | | | |
| #04 | VEX | W08 | 2011-Oct-05 02:32 | Oct-05 20:10 | ICME | 07:04 | −07:01 | 1166 | 700 | |
| #05 | VEX | W09 | 2011-Oct-15 08:26 | Oct-16 01:00 | ICME† | 05:02 | −05:27 | 954 | 665 | |
| #06 | VEX | W10 | 2011-Nov-04 15:09 | Nov-05 03:45 | ICME† | 01:33 | −11:05 | 1071 | 940 | 780 |
| #07 | VEX | W20 | 2012-Mar-04 10:34 | Mar-05 18:30 | ICME | 11:43 | −02:07 | 842 | 535 | |
| #08 | VEX | W21 | 2012-Mar-05 12:28 | Mar-06 08:25 | ICME | 08:14 | −13:57 | 1447 | 850 | |
| #09 | VEX | W22 | 2012-Mar-07 04:37 | VOID | | | | | | |
| #10 | VEX | W23 | 2012-Mar-12 13:47 | NO DATA | | | | | | |
| #11 | VEX | W31 | 2012-Aug-09 11:33 | Aug-10 19:30 | ICME° | 02:15 | 02:04 | 503 | 460 | |
| #12 | VEX | W47 | 2013-Oct-26 11:07 | Oct-27 11:15 | ICME† * | 02:03 | −07:17 | 712 | 650 | 450 |
| #13 | VEX | W48 | 2013-Oct-27 12:35 | | | | | | | |
| #14 | VEX | W56 | 2014-Feb-17 04:16 | VOID | | | | 821 | | |
| #15 | VEX | W58 | 2014-Jul-27 16:01 | Jul-29 09:00 | ICME† | 00:07 | 06:44 | 419 | 420 | |
| #16 | ACE | W43 | 2013-Jul-11 01:05 | Jul-12 16:30 | ICME† | −02:27 | −07:03 | 555 | 590 | 440 |
| #17 | ACE | W49 | 2013-Oct-29 07:15 | Oct-30 18:45 | ICME° | 03:54 | −18:29 | 854 | 760 | 360 |
| #18 | ACE | W55 | 2014-Feb-13 04:51 | Feb-15 12:40 | ICME† | 24:42 | 02:11 | 865 | 480 | 470 |
| #19 | ACE | W56 | 2014-Feb-17 04:16 | Feb-19 03:10 | ICME† | 15:16 | −05:03 | 821 | 555 | 480 |
| #20 | ST-A | W01 | 2011-May-19 11:50 | May-21 09:20 | ICME | 21:59 | 00:16 | 962 | 495 | 470 |
| #21 | ST-A | W06 | 2011-Sep-06 23:33 | Sep-08 16:05 | ICME† | 00:55 | −14:09 | 690 | 675 | 360 |
| #22 | ST-A | W14 | 2011-Dec-31 16:27 | NO DATA | | | | | | |
| #23 | ST-A | W15 | 2012-Jan-02 18:28 | Jan-04 16:40 | ICME† * | 10:17 | 02:16 | 612 | 475 | 390 |
| #24 | ST-A | W16 | 2012-Jan-03 04:52 | | * | | | | | |
| #25 | ST-A | W17 | 2012-Jan-03 17:56 | | | | | | | |
| #26 | ST-A | W25 | 2012-May-08 08:39 | May-10 21:45 | ICME | 34:36 | 14:31 | 879 | 380 | 310 |
| #27 | ST-A | W26 | 2012-May-17 12:09 | May-18 12:40 | ICME† | 05:34 | −26:26 | 1344 | 1035 | 770 |
| #28 | ST-A | W40 | 2013-May-01 05:45 | May-02 21:00 | ICME† | −07:33 | −10:16 | 529 | 630 | 510 |
| #29 | ST-A | W44 | 2013-Aug-20 12:41 | Aug-22 07:05 | ICME† | 15:11 | −10:40 | 975 | 625 | 540 |
| #30 | ST-A | W59 | 2014-Aug-09 19:39 | Aug-11 09:00 | ICME† | −12:56 | −14:45 | 518 | 695 | 490 |
| #31 | ST-B | W10 | 2011-Nov-04 15:09 | Nov-06 05:10 | ICME† | 13:02 | −15:29 | 1071 | 705 | |
| #32 | ST-B | W11 | 2011-Nov-14 02:06 | Nov-17 02:05 | IP† | 16:37 | 14:51 | 516 | 395 | |
| #33 | ST-B | W41 | 2013-May-19 18:53 | May-22 22:50 | ICME | −08:22 | 18:27 | 341 | 380 | |
| #34 | ST-B | W45 | 2013-Sep-05 13:39 | Sep-07 22:00 | IP† | 14:21 | 04:56 | 612 | 455 | |
| #35 | ST-B | W46 | 2013-Sep-12 23:36 | Sep-15 14:00 | ICME† | 12:23 | 13:05 | 493 | 395 | |
| #36 | ST-B | W59 | 2014-Aug-09 19:39 | Aug-11 05:50 | ICME† | −19:21 | −21:06 | 518 | 810 | 620 |

† Shock is listed in public catalogs.
* ICME interacts with the previous one.
° There is no sheath preceding the magnetic ejecta.

hereafter (right panel of Fig. 1). There are two IPs. Among the 29 ICMEs, three ICMEs are not resolved at the targets because they interacted with other ICMEs between MESSENGER and the targets. Table 2 gathers for each pair, observed arrival times, time mismatches from predicted arrival times, and velocities.

Finally the False category is empty, which requires some comments. An interplanetary shock followed, or not followed, by an ICME was identified ±24 h from $t_{predVmes}$ and/or $t_{predV500}$ for each pair where interplanetary magnetic field measurements are available. ICMEs are observed at the target with large time delays with regard to predicted times (columns $\Delta t_{Vmess}$ and $\Delta t_{V500}$ in Table 1) in several cases (larger than 20 h for pairs #02, #18, #20, #26, #27, and #36). Pair #02 corresponds to a fast ICME: both $\overline{v}_{SunMess}$ and $\overline{v}_{MessTar}$ are high. A default velocity of 500 km s$^{-1}$ leads for that case to a large $\Delta t_{V500}$ value. ICME shocks are strongly decelerated between MESSENGER and the targets for pairs #18, #20, and #27 leading to a high $\Delta t_{Vmess}$ value. $\overline{v}_{MessTar}$ and $v_{Tar}$ in pair #26 are close to each other: $\overline{v}_{SunMess}$ might be overestimated. Pair #36 observations are detailed in Section 5.1.

Beyond Mercury's orbit, CME-CME interactions have implications for ICME propagation (Lugaz et al., 2012). It might concern CMEs following each other at Mercury (in pairs #01-#02; #07-#08; #12-#13; #23-#24-#25). In two cases we were not able to properly identify different ICMEs at the targets (#12-#13; #23-#24-#25). We take into account only one shock for each of these two cases.

Identified ICMEs and IPs are mentioned in a catalog (see Sect. 2) for 19 of 28 cases (cf. Table 2). As for the 9 other events of the 28, ICMEs have various aspects, from the textbook case to a very short magnetic ejecta. We also mention two ICMEs (pairs #11 and #17) without a sheath. It is quite obvious that the CME-driven shock is larger in longitudinal direction than the ICME itself (see Fig. 1 in Kilpua et al., 2017). ENLIL simulations show that for the two IP events STEREO-B is on the edge of an ICME that went through MESSENGER earlier. IPs are related to ICMEs and we keep the two events in our study of the ICME shock deceleration. These events are important for space weather alerts as, at Earth and probably elsewhere, the sheath of the ICME can be more effective than the ICME itself (e.g., Kilpua et al., 2017; Bocchialini et al., 2018).

We emphasize here that besides Propagation Tool predictions, timing considerations, in situ observations, and simulations, there is no certainty that the ICME observed at MESSENGER is the one observed at the target.

However this is not surprising to have a high number of matches as ICMEs propagate radially, and we also use a loose criterion for the ICME identification. Möstl et al. (2017) found that 25–35% of 1335 ICME arrivals were correctly predicted, assuming a constant speed and propagation direction and a longitudinal extent of 60°. Having MESSENGER as a starting point rather than the Sun can explain the higher rate of correct predictions, because our study involves only ICMEs which propagate inside the ecliptic plane. We also avoid cases when drastic changes in CME propagation occur close to the Sun (Möstl et al., 2015).

Figure 1 presents a Correct-pair sample (left part of the figure) and a Void-pair sample (right part). $t_{obsMESS}$, $t_{predV500}$, $t_{predVmes}$, and $t_{obsTAR}$ are marked by vertical dashed lines (blue, red, green and violet, respectively).

The Correct-pair sample has STEREO-A as a target. Over the 60 h presented in Figure 1, one can notice a single shock observed in both, the magnetic field and the bulk flow velocity (panels a–c). The shock arrival time (22 August 2002 07:05) is $t_{obsTAR}$ (see vertical violet line). Later on (23 August 02:00 UT), one can notice the arrival of the ICME's magnetic ejecta, i.e. the smooth part of the magnetic field. $t_{obsTAR}$ is observed later than $t_{predVmes}$ and earlier than $t_{predV500}$, making an identification of $t_{obsTAR}$ easy. The large gap (26 h) observed between $t_{predVmes}$ and $t_{predV500}$ results from the large ICME shock velocity estimated at MESSENGER ($\overline{v}_{SunMess} = 975$ km s$^{-1}$) compared to the Propagation Tool default velocity (500 km s$^{-1}$). The difference between $\overline{v}_{SunMess}$ and $v_{Tar}$ (540 km s$^{-1}$) can result from a strong deceleration between MESSENGER and STEREO-A or from a bad estimation of the velocity at MESSENGER. Finding $\overline{v}_{MessTar}$ (625 km s$^{-1}$) between $\overline{v}_{SunMess}$ and $v_{Tar}$ supports the deceleration assumption.

The Void pair sample has VEX as a target. The three components and the magnitude of the magnetic field are plotted in panels d and e, respectively. The VEX-Venus distance is plotted in panel f. In the vicinity of the three periapsis passages, $B$ fluctuates and $|\boldsymbol{B}|$ intensifies (Fig. 1d and e), obviously due to bow shock crossings. The intensification observed during bow shock outbound is usually the largest (7 and 9 March 2012 periapsis). In the 8 March periapsis case, there is also a large $|\boldsymbol{B}|$ increase at the beginning of the fluctuation period that can correspond to the bow shock inbound. Even looking closer to the data it is not clear if it results from an interplanetary shock or from a bow shock crossing. It occurs close to the predicted shock arrival times ($t_{predVmes}$ and $t_{predV500}$).

Farther from the periapsis, VEX can be considered to be inside the interplanetary medium. There is a remarkable shock visible on 7 March at 13:15 UT, followed by an ICME magnetic ejecta which starts at 20:00 UT. The timing of this shock leads to a mean ICME velocity $\overline{v}_{MessTar}$ of about 1950 km s$^{-1}$, between MESSENGER and VEX, which is very high. As we are not certain that an interplanetary shock reached Venus during the March 8 periapsis, and that the 7 March shock corresponds to the ICME seen at MESSENGER, this pair is classified as Void.

## 4 ICME acceleration and deceleration in the interplanetary medium

We considered in that study the 28 ICME and IP events (cf. Table 2). Comparing the average velocities $\overline{v}_{SunMess}$ (estimated in Winslow et al., 2015), $\overline{v}_{MessTar}$, and $v_{Tar}$ allow us to study deceleration ($\overline{v}_{SunMess} > \overline{v}_{MessTar}$; $\overline{v}_{MessTar} > v_{Tar}$) or acceleration in the interplanetary medium. Mean velocity values for different subsets are gathered in Table 3.

When considering the 15 pairs for which $v_{Tar}$ is available, one can notice that $v_{Tar}$ is systematically lower than $\overline{v}_{MessTar}$. The mean $v_{Tar}$ value (653 km s$^{-1}$ on average, cf. Table 3) is lower than the mean $\overline{v}_{MessTar}$ (493 km s$^{-1}$), by 160 km s$^{-1}$: ICME shocks are slowing down between MESSENGER and the targets. We also note that $\overline{v}_{SunMess}$ is larger than $\overline{v}_{MessTar}$ in 22 of 28 cases, and by 171 km s$^{-1}$ on average: ICME shocks generally slow down between the solar corona and the targets.

We detail now the six cases where $\overline{v}_{MessTar} > \overline{v}_{SunMess}$. For three pairs (#15, #16, and #33), $\overline{v}_{MessTar}$ exceeds $\overline{v}_{SunMess}$ by less than 40 km s$^{-1}$. These cases are not certain cases of ICME acceleration as these value can be explained by an uncertainty in $\overline{v}$: assuming a rigid cone structure of the shock in the radial propagation is probably not realistic. However, #15 and #33 pairs have the lowest $\overline{v}_{SunMess}$ values of our dataset (419 and 341 km s$^{-1}$). Gopalswamy et al. (2001a) noted that slow ICMEs have a larger probability to be accelerated than the fast ones. In the three other pairs (#28, #30, and #36) $\overline{v}_{MessTar}$ is larger than $\overline{v}_{SunMess}$ by more than 100 km s$^{-1}$. However, in those cases $\overline{v}_{MessTar}$ is also larger than $\overline{v}_{Tar}$ by more than 100 km s$^{-1}$ which is indicative of a deceleration between MESSENGER and the targets. In these three cases, $\overline{v}_{SunMess}$ might be underestimated because of a wrong CME-ICME association, thus making ICME acceleration questionable. Bocchialini et al. (2018) discusses the difficulties of correctly associating CMEs with ICMEs. There is no definitive evidence of ICME shock acceleration beyond Mercury's orbit in these six events.

Figure 2 presents velocity variations as a function of the Sun-Mercury distance for the slow ICMEs ($\overline{v}_{SunMess} <$ 600 km s$^{-1}$, top panel) and the fast ICMEs ($\overline{v}_{SunMess} >$ 600 km s$^{-1}$, bottom panel). In the top panel, one can note that the six cases when $\overline{v}_{SunMess} < \overline{v}_{MessTar}$ (meaning that the ratio of velocities is less than 1) are included in the nine slow ICME cases when an ICME acceleration by the surrounding

**Table 3.** Average velocity values for different data sets. The number of included pairs is listed under "size".

| Data set | | $\overline{v}_{SunMess}$ | $\overline{v}_{MessTar}$ | $v_{Tar}$ |
|---|---|---|---|---|
| Name | Size | km s$^{-1}$ | km s$^{-1}$ | km s$^{-1}$ |
| VEX | 10 | 1103 | 831 | n/a |
| 1 AU | 18 | 731 | 585 | n/a |
| ALL | 28 | 864 | 673 | n/a |
| | | Only events with $v_{Tar}$ | | |
| 1 AU | 13 | 779 | 631 | 474 |
| ALL | 15 | 794 | 653 | 493 |

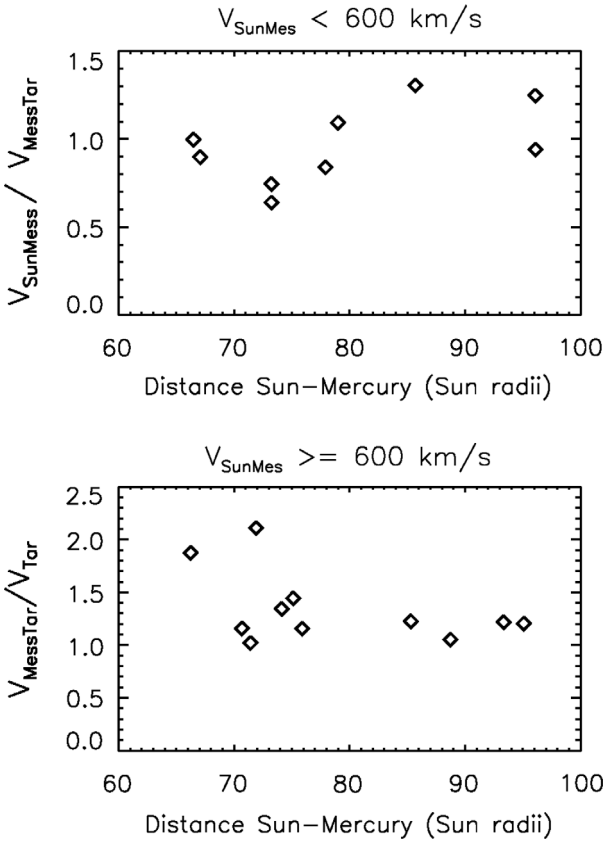


**Fig. 2.** ICME velocity evolution vs. Mercury-Sun distance for ICMEs observed at MESSENGER with a velocity lower than 600 km s$^{-1}$ (top panel) and larger than 600 km s$^{-1}$ (bottom panel). Note that plots are ratio of average velocities (top panel) and ratio of average to in situ velocity (bottom panel).

interplanetary material is more probable. The lowest ratios are observed within 75 $R_\odot$ (≈0.35 AU). Major speed changes are expected to occur close to the Sun, especially within 50 $R_\odot$ (Liu et al., 2016). If both ICME associations at MESSENGER and at the targets are correct, the region with positive acceleration can extent to 75 $R_\odot$. Looking at the influence of the distance of Mercury to the Sun on the $\overline{v}_{MessTar}/v_{Tar}$ ratio for the fast ICMEs (bottom panel of Fig. 2), strongest deceleration cases are observed below 80 $R_\odot$ (≈0.37 AU), when the distance of Mercury to the targets is near maximum due to Mercury's highly elliptical orbit.

**Table 4.** Observed versus predicted impact time of the 28 ICME shocks (mean values and standard deviation values).

| $\Delta t$ | Mean h | $\sigma$ h |
|---|---|---|
| $t_{obsTAR} - t_{predV500}$ | −5.5 | 12.2 |
| $t_{obsTAR} - t_{predVmes}$ | 6.5 | 11.4 |

In order to study shock deceleration between VEX and 1 AU, we sort Correct pairs into two subsets: the VEX subset (10 VEX pairs) and the 1 AU subset (18 STEREO-A and B, and ACE pairs). $\overline{v}_{MessTar}$ is much higher on average in the VEX subset (831 km s$^{-1}$) than in the 1 AU subset (585 km s$^{-1}$). This alone does not confirm a deceleration of ICMEs between VEX and 1 AU because also $\overline{v}_{SunMess}$ for the VEX subset is on average ≈370 km s$^{-1}$ higher than in the 1 AU subset (1103 km s$^{-1}$ vs. 731 km s$^{-1}$).

A statistics on the differences between the observed arrival time $t_{obsTAR}$ and the predicted arrival times ($t_{predV500}$ and $t_{predVmes}$) is presented in Table 4, for all Correct pairs. According to the propagation velocity analysis, the standard deviation of the propagation time is quite high (11–12 h). The standard deviation is lower than the 16.6 h found in Möstl et al. (2017). ICME major speed changes occur within 30 $R_\odot$ (Liu et al., 2016). Avoiding that area by starting from Mercury's orbit might explain the lower standard deviation found in our data set.

The negative mean value of $t_{obsTAR} - t_{predV500}$ shows that the default velocity of the Propagation Tool leads to a delay of −5.5 h on average. The slowing down of the ICME after passing MESSENGER leads to an error of 6.5 h on average in the predicted arrival time based on $t_{predVmes}$. Considering the absolute error, the default velocity and $\overline{v}_{SunMess}$ predict the arrival time with a similar precision.

## 5 Events involving multiple solar system bodies

Three ICMEs (#10, #56, and #59) at MESSENGER are paired with more than one target (see Table 2). ICME #10 is paired with VEX and STEREO-B, and ICME #59 is paired with both STEREO spacecraft, as shown in Figure 3 and detailed hereafter.

### 5.1 ICME W#10: Pairs #06 and #31

Figure 4 shows data from VEX (panels a–c) and STEREO-B (panels d and e). At VEX (respectively at STEREO-B) the arrival time of the ICME shock is marked by a dashed red (blue, resp.) line in panel b (e, resp.). VEX encounters the shock near its periapsis. The ICME is seen as an organized and intense magnetic field lasting roughly one day (6 November 2011). The picture is complicated by the proximity to Venus. At STEREO-B, the ICME lasts two days (7 and 8 November). The magnetic field is more organized than at VEX.

It is worth noticing that considering radial propagation between VEX and STEREO-B, the ICME shock velocity is about 590 km s$^{-1}$, which is lower than $\overline{v}_{MessTar}$ at VEX

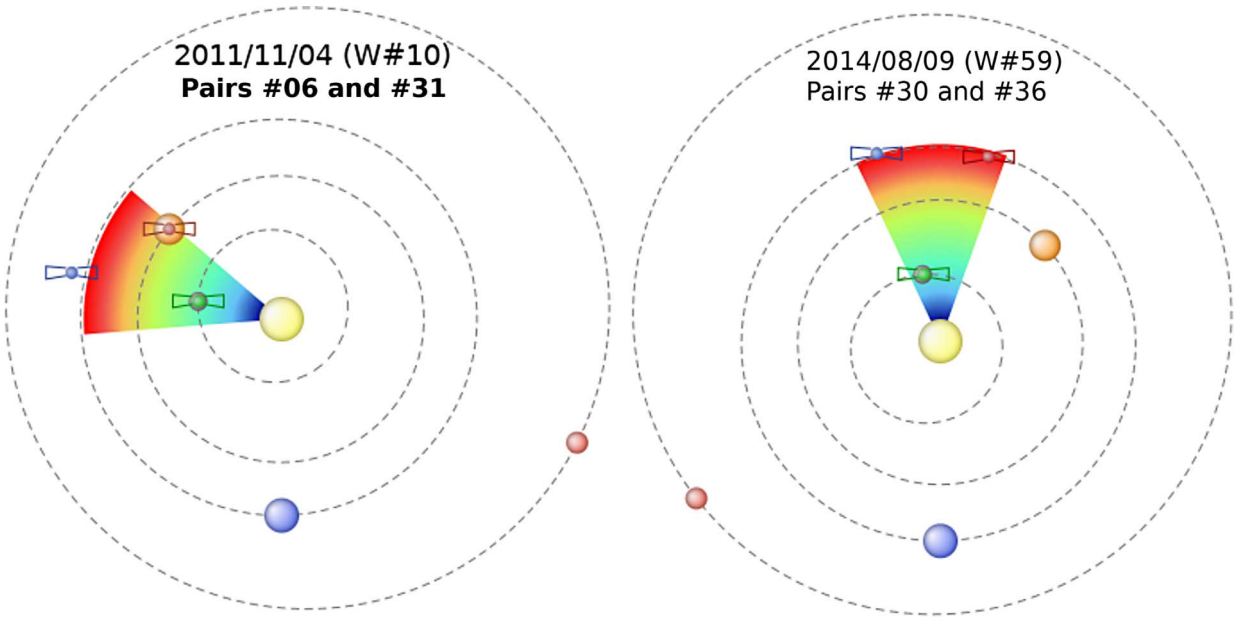


**Fig. 3.** View of the inner solar system for ICMEs W#10 (left) and W#59 (right). The Sun is in the centre. The four inner planet positions are marked by filled circles and their orbits are indicated by dashed lines. The MESSENGER and target spacecraft positions are sketched as well. An ICME's trajectory is materialized by the colored cone (45° aperture). Colors indicate the distance to the Sun (from 0 AU, blue, to 1 AU, red). Figure extracted from the CDPP Propagation Tool.

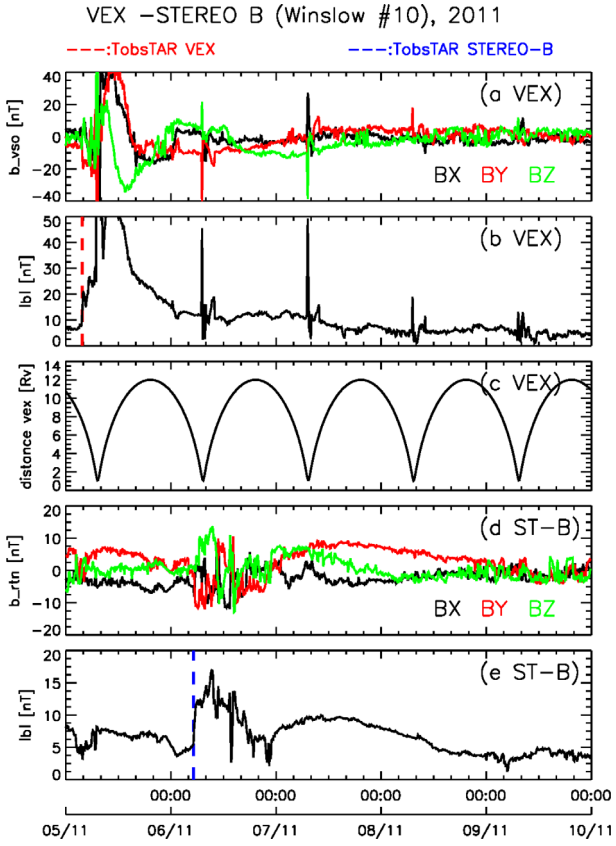


**Fig. 4.** Winslow #10 ICME observed at VEX (pair #06, three top panels) and STEREO-B (pair #31, two bottom panels). Panels a and d: three components of the magnetic field (***B***); panels b and e: ***B*** intensity; panel c: VEX-Venus distance.

(940 km $s^{-1}$) and at STEREO-B (705 km $s^{-1}$), and lower than $v_{Tar}$ at VEX (780 km $s^{-1}$). In that case, it seems likely that the same ICME is observed by VEX and STEREO-B. The different velocities indicate that the ICME's radial velocity is decreasing from MESSENGER to VEX and further decreasing from VEX to STEREO-B. Even if the solar wind velocities are not continuously available at STEREO-B, the data indicate that the shock arrives with a velocity of $v_{Tar} \approx 620$ km $s^{-1}$. This is quite close to the 590 km $s^{-1}$ mean velocity obtained between VEX and STEREO-B. The slightly lower value can be explained by the geometry of the ICME: VEX and STEREO-B are not radially aligned.

### 5.2 ICME W#59: pairs #30 and #36

Figure 5 presents the same ICME seen at STEREO-A (left) and at STEREO-B (right). The ICME is easily identified in STEREO-A data. Sudden IMF strength and solar wind velocity increases mark the shock arrival (11 August 2014 09:00 UT). The ICME's sheath lasts about 1 day. Then, the ICME's magnetic ejecta is observed from 12 August 08:00 to 13 August 20:00. The ICME displays a remarkably stable and rotating IMF and low solar wind density. One can also note the gradual decrease of both IMF strength and solar wind velocity. These properties correspond to a magnetic cloud.

The picture is more complicated at STEREO-B: it is difficult to identify a shock arrival time. We choose 11 August 05:50 because of concomitant jumps in IMF strength and solar wind velocity. The ICME magnetic ejecta starts on 11 August at 09:00. The IMF is less structured and fluctuates more contrary to STEREO-A observations. Furthermore, the solar wind density is low for a few hours before the IMF's ending on 14 August, 10:00.

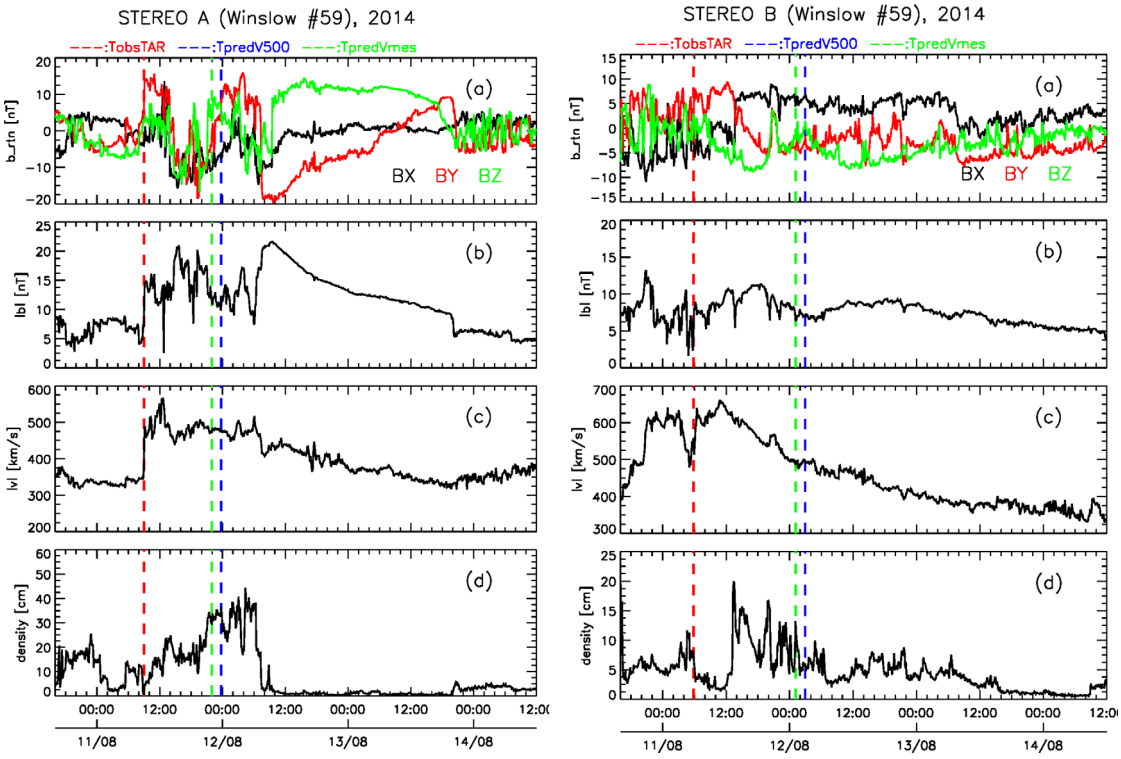


**Fig. 5.** Winslow #59 ICME observed at STEREO-A (pair #30, left panels) and STEREO-B (pair #36, right panels). Panel a: three components of the magnetic field (***B***); panel b: ***B*** intensity; panel c: plasma bulk flow velocity; panel d: plasma density.

A striking feature is the difference in observations from STEREO-A and B: the ICME magnetic ejecta is observed at STEREO-B earlier than at STEREO-A, even though the latter is closer to the Sun. Accordingly, ICME and shock velocities are larger at STEREO-B (>620 km $s^{-1}$) than at STEREO-A (<500 km $s^{-1}$). However, the magnetic ejecta signature is very confused at STEREO-B.

It is thus reasonable to ask whether the two spacecraft observe the same ICME. Looking at the Sun, STEREO-A and B coronagraphs observe only one CME on 8 August, and none on 9 or 10 August (https://cor1.gsfc.nasa.gov/catalog/cme/2014/HongXie_COR1_preliminary_event_list_2014-08.html). This CME, also seen in SOHO/LASCO coronagraphs, is listed as the source CME of the ICME observed at MESSENGER. LASCO observes only two minor events prior and after this CME (https://cdaw.gsfc.nasa.gov/CME_list/UNIVERSAL/2014_08/univ2014_08.html). They come from a different source location. Due to the weak solar activity during those days, it is unlikely that STEREO-A and B were hit by two different ICMEs. We thus believe that STEREO-A is encountering the ICME at a place where it is still well structured while the ICME part encountered by STEREO-B experienced more interactions with the ambient solar wind. The larger velocity seen at STEREO-B might be the result of an interaction with a high-speed stream in the ambient solar wind that is affecting only the part of the ICME which is finally sweeping over STEREO-B.

This example demonstrates the azimuthal variations observed in an ICME at two different locations which are separated by less than 40° in azimuthal direction. This finding agrees with a study by Good & Forsyth (2016) who noticed a reduced number of ICMEs observed by two spacecraft when the angular separation is larger than 30°.

## 6 Conclusion

Based on 61 ICME events observed at MESSENGER, the Propagation Tool predicts an impact at VEX, STEREO-A, STEREO-B, and ACE in 36 cases. Out of these, 28 events are suitable for a comparison of $\overline{v}_{\mathrm{SunMess}}$ and $\overline{v}_{\mathrm{MessTar}}$. ICME shocks are clearly decelerated in 22 cases, unlikely accelerated in three cases, and in three cases the velocity remains almost constant. The same ICME observed at MESSENGER is paired with two different targets in three cases. Different signatures of the same ICME are observed at 40° angular separation.

In the 13 pairs with available $v_{\mathrm{Tar}}$, ICME shock velocities always decrease between MESSENGER and the targets ($\overline{v}_{\mathrm{MessTar}} > v_{\mathrm{Tar}}$). The average speed difference is ≈160 km $s^{-1}$. With respect to the mean Sun-Mercury transit velocity, the ICME speed decreases by about 300 km $s^{-1}$ on average ($\overline{v}_{\mathrm{SunMess}} - v_{\mathrm{Tar}}$). Freiherr von Forstner et al. (2018) studied a similar number of events (15 vs. 13 in our study) with similar mean $v_{\mathrm{Tar}}$ values (474 vs. 475 km $s^{-1}$). They noted a 170 km $s^{-1}$ average deceleration between the solar corona and 1 AU and a 60 km $s^{-1}$ average deceleration between 1 and 1.5 AU (Mars orbit). Our results show that ICME deceleration is still strong between Mercury and 1 AU. We believe the deceleration observed in the present study results from the accumulation of the solar wind plasma upstream of the ICME.

Emission of (magneto)hydrodynamic waves in this collisionless environment causes the drag between ICME and solar wind (Cargill et al., 1996; Vršnak et al., 2013), as already observed (Lindsay et al., 1999; Gopalswamy et al., 2000).

We do not follow ICMEs all the way between MESSENGER and the targets. Our ICME/ICME associations rely on timing, ICME identification and on global simulations. Our dataset suggests that ICME shock deceleration between MESSENGER and the targets is the common case. There is no convincing observations of ICME shock positive acceleration since cases with $\overline{v}_{\mathrm{MessTar}} > v_{\mathrm{Tar}}$ are not part of our dataset. Potentially most accelerated ICME shocks ($\overline{v}_{\mathrm{SunMess}}/\overline{v}_{\mathrm{MessTar}} < 0.9$) and most decelerated shocks ($\overline{v}_{\mathrm{MessTar}}/v_{\mathrm{Tar}} > 1.8$) are observed at MESSENGER when Mercury is located between 65 and 80 $R_{\odot}$ (≈0.30 and ≈0.37 AU). Major speed changes can thus occur in a larger region than the 50 $R_{\odot}$ limit found by Liu et al. (2016).

Evidence of ICME deceleration between VEX and STEREO-B is found based on ICMEs observed by MESSENGER, VEX and STEREO-B. Our results suggest that ICME deceleration would occur as long as ICMEs propagate faster than the surrounding solar wind as noted by Witasse et al. (2017) at a larger distance.

We conclude that the CDPP Propagation Tool is helpful in studying ICME propagation between bodies in the inner solar system. The predicted arrival time is, on average, correct within a $-5.5 \pm 12.2$ h margin. An ICME shock is observed at a target in 31 of 36 pair predictions. The lack of events classified as False follows from our choice to reject observations inside Mercury's orbit where drastic changes in ICME parameters are more frequent. The proportion of ICMEs observed at 1 AU that have not been observed at MESSENGER is left for a further study. By means of real-time in situ data obtained between the Sun and the Earth, uncertainties in shock arrival times can be reduced and predictions for ICME propagation can be improved in general. In our study the shortest propagation time between Mercury and VEX is about 8 h and 24 h between Mercury and 1 AU. Using spacecraft like MESSENGER as monitor for extreme solar events shortens the time to communicate an updated alert status as compared to observing directly the activity on the solar surface. However, it enables a more accurate prediction of propagation path and geoeffectiveness of a potentially hazardeous ICME. Our study demonstrates the utility of having in situ measurements between the Sun and Earth in an operational space weather context. In the future, ESA's Solar Orbiter, ESA-JAXA's Bepi-Colombo, and NASA's Parker Solar Probe missions will provide more opportunities to observe ICMEs at different locations in the inner solar system.

*Acknowledgements.* This study has been carried out with the support of the Europlanet 2020 research infrastructure. Europlanet 2020 RI has received funding from the European Union's Horizon 2020 Research and Innovation Program under grant agreement No. 654208. Authors also acknowledge support of GACR grants No. 18-05285S and 17-08722S, and of the Praemium Academiae Award. V.K. acknowledges support by an appointment to the NASA postdoctoral program at the NASA Goddard Space Flight Center administered by Universities Space Research Association under contract with NASA and the Czech Science Foundation grant 17-06818Y. Authors thank A. Opitz for fruitful discussions at the beginning of this work. Data analysis was performed with the AMDA science analysis system provided by the Centre de Données de la Physique des Plasmas (CDPP) supported by CNRS, CNES, Observatoire de Paris and Université Paul Sabatier, Toulouse. All the data used for this study are publicly available on the AMDA website (http://amda.cdpp.eu/). We thank the ACE SWEPAM and ACE MAG instrument teams and the ACE Science Center for providing the ACE data. We thank the STEREO IMPACT/MAG and PLASTIC instrument teams. MESSENGER MAG data are available from NASA's Planetary Data System. The authors acknowledge the Principal Investigator T. Zhang (OAW, Graz) of the MAG instrument onboard the VEX mission for providing datasets in the archive. Datasets of the VEX MAG instrument have been downloaded from the ESA Planetary Science Archive (http://archives.esac.esa.int/psa). The editor thanks Olga Malandraki and an anonymous referee for their assistance in evaluating this paper.

## References

Bocchialini K, Grison B, Menvielle M, Chambodut A, Cornilleau-Wehrlin N, et al. 2018. Statistical analysis of solar events associated with storm sudden commencements over one year of solar maximum during cycle 23: Propagation from the Sun to the Earth and effects. *Sol Phys* **293**: 75. DOI: 10.1007/s11207-018-1278-5.

Brueckner GE, Delaboudiniere J-P, Howard RA, Paswaters SE, St. Cyr OC, Schwenn R, Lamy P, Simnett GM, Thompson B, Wang D. 1998. Geomagnetic storms caused by coronal mass ejections (CMEs): March 1996 through June 1997. *Geophys Res Lett* **25(15)**: 3019–3022. DOI: 10.1029/98GL00704.

Burlaga L, Sittler E, Mariani F, Schwenn R. 1981. Magnetic loop behind an interplanetary shock - Voyager, Helios, and IMP 8 observations. *J Geophys Res* **86**: 6673–6684. DOI: 10.1029/JA086iA08p06673.

Cane HV, Richardson IG. 2003. Interplanetary coronal mass ejections in the near-Earth solar wind during 1996-2002. *J Geophys Res (Space Phys)* **108**: 1156. DOI: 10.1029/2002JA009817.

Cargill PJ, Chen J, Spicer DS, Zalesak ST. 1996. Magnetohydrodynamic simulations of the motion of magnetic flux tubes through a magnetized plasma. *J Geophys Res (Space Phys)* **101(A3)**: 4855–4870. DOI: 10.1029/95JA03769.

Davis CJ, Davies JA, Lockwood M, Rouillard AP, Eyles CJ, Harrison RA. 2009. Stereoscopic imaging of an Earth-impacting solar coronal mass ejection: A major milestone for the STEREO mission. *Geophys Res Lett* **36(8)**: L08102. DOI: 10.1029/2009GL038021.

Freiherr von Forstner JL, Guo J, Wimmer-Schweingruber RF, Hassler DM, Temmer M, et al. 2018. Using Forbush decreases to derive the transit time of ICMEs propagating from 1 AU to Mars. *J Geophys Res (Space Phys)* **123**: 39–56. DOI: 10.1002/2017JA024700.

Gonzalez WD, Echer E, Clua-Gonzalez AL, Tsurutani BT. 2007. Interplanetary origin of intense geomagnetic storms (Dst < −100 nT) during solar cycle 23. *Geophys Res Lett* **34**: L06101. DOI: 10.1029/2006GL028879.

Good SW, Forsyth RJ. 2016. Interplanetary coronal mass ejections observed by MESSENGER and Venus Express. *Solar Phys* **291(1)**: 239–263. DOI: 10.1007/s11207-015-0828-3.

Gopalswamy N, Lara A, Lepping RP, Kaiser ML, Berdichevsky D, St. Cyr OC. 2000. Interplanetary acceleration of coronal mass ejections. *Geophys Res Lett* **27(2)**: 145–148. DOI: 10.1029/1999GL003639.

Gopalswamy N, Lara A, Yashiro S, Kaiser ML, Howard RA. 2001a. Predicting the 1-AU arrival times of coronal mass ejections. *J Geophys Res (Space Phys)* **106(A12)**: 29207–29217. DOI: 10.1029/2001JA000177.

Gopalswamy N, Yashiro S, Kaiser ML, Howard RA, Bougeret JL. 2001b. Radio signatures of coronal mass ejection interaction: Coronal mass ejection cannibalism? *ApJ* **548**: L91–L94. DOI: 10.1086/318939.

Gosling JT, Pizzo V, Bame SJ. 1973. Anomalously low proton temperatures in the solar wind following interplanetary shock waves – evidence for magnetic bottles? *J Geophys Res* **78(13)**: 2001–2009. DOI: 10.1029/JA078i013p02001.

Jian LK, Russell CT, Luhmann JG, Galvin AB. 2018. STEREO observations of interplanetary coronal mass ejections in 2007–2016. *ApJ* **855(2)**: 114. DOI: 10.3847/1538-4357/aab189.

Kaiser ML, Kucera TA, Davila JM, St. Cyr OC, Guhathakurta M, Christian E. 2008. The STEREO mission: an introduction. *Space Sci Rev* **136(1)**: 5–16. DOI: 10.1007/s11214-007-9277-0.

Kilpua E, Koskinen HEJ, Pulkkinen TI. 2017. Coronal mass ejections and their sheath regions in interplanetary space. *Living Rev Sol. Phys* **14(1)**: 5. DOI: 10.1007/s41116-017-0009-6.

Lindsay GM, Luhmann JG, Russell CT, Gosling JT. 1999. Relationships between coronal mass ejection speeds from coronagraph images and interplanetary characteristics of associated interplanetary coronal mass ejections. *J Geophys Res (Space Phys)* **104(A6)**: 12515–12523. DOI: 10.1029/1999JA900051.

Liu Y, Davies JA, Luhmann JG, Vourlidas A, Bale SD, Lin RP. 2010. Geometric triangulation of imaging observations to track coronal mass ejections continuously out to 1 AU. *Astrophys J Lett* **710(1)**: L82. DOI: 10.1088/2041-8205/710/1/L82.

Liu Y, Richardson JD, Belcher JW. 2005. A statistical study of the properties of interplanetary coronal mass ejections from 0.3 to 5.4 AU. *Planet Space Sci* **53**: 3–17. DOI: 10.1016/j.pss.2004.09.023.

Liu YD, Hu H, Wang C, Luhmann JG, Richardson JD, Yang Z, Wang R. 2016. On sun-to-earth propagation of coronal mass ejections: II. slow events and comparison with others. *Astrophys J Suppl Ser* **222(2)**: 23. DOI: 10.3847/0067-0049/222/2/23.

Lugaz N, Farrugia CJ, Davies JA, Mstl C, Davis CJ, Roussev II, Temmer M. 2012. The deflection of the two interacting coronal mass ejections of 2010 May 23–24 as revealed by combined in situ measurements and heliospheric imaging. *ApJ* **759(1)**: 68. DOI: 10.1088/0004-637X/759/1/68.

Malandraki OE, Lario D, Lanzerotti LJ, Sarris ET, Geranios A, Tsiropoula G. 2005. October/November 2003 ICMEs: ACE/EPAM solar energetic particle observations. *J Geophys Res* **110**: **A09S06**. DOI: 10.1029/2004JA010926. Special Section: Violent Sun-Earth connection events of October-November 2003.

Malandraki OE, Marsden RG, Tranquille C, Forsyth RJ, Elliott HA, Lanzerotti LJ, Geranios A. 2007. Energetic particle observations by *Ulysses* during the declining phase of solar cycle 23. *J Geophys Res*, **112**, **A06111**. DOI: 10.1029/2006JA011876.

Manchester W, Kilpua EKJ, Liu YD, Lugaz N, Riley P, Török T, Vršnak B. 2017. The physical processes of CME/ICME evolution. *Space Sci Rev* **212(3)**: 1159–1219. DOI: 10.1007/s11214-017-0394-0.

Möstl C, Isavnin A, Boakes PD, Kilpua EKJ, Davies JA, et al. 2017. Modeling observations of solar coronal mass ejections with heliospheric imagers verified with the heliophysics system observatory. *Space Weather* **15(7)**: 955–970. DOI: 10.1002/2017SW001614.

Möstl C, Rollett T, Frahm RA, Liu YD, Long DM, et al. 2015. Strong coronal channelling and interplanetary evolution of a solar storm up to Earth and Mars. *Nat Commun* **6**: 7135. DOI: 10.1038/ncomms8135.

Odstrcil D, Pizzo VJ. 1999. Distortion of the interplanetary magnetic field by three-dimensional propagation of coronal mass ejections in a structured solar wind. *J Geophys Res* **104**: 28225–28240. DOI: 10.1029/1999JA900319.

Odstrcil D, Pizzo VJ. 2009. Numerical heliospheric simulations as assisting tool for interpretation of observations by STEREO heliospheric imagers. *Sol Phys* **259**: 297–309. DOI: 10.1007/s11207-009-9449-z.

Prise AJ, Harra LK, Matthews SA, Arridge CS, Achilleos N. 2015. Analysis of a coronal mass ejection and corotating interaction region as they travel from the Sun passing Venus, Earth, Mars, and Saturn. *J Geophys Res (Space Phys)* **120**: 1566–1588. DOI: 10.1002/2014JA020256.

Richardson IG, Cane HV. 1993. Signatures of shock drivers in the solar wind and their dependence on the solar source location. *J Geophys Res (Space Phys)* **98(A9)**: 15295–15304. DOI: 10.1029/93JA01466.

Richardson IG, Cane HV. 2010. Near-Earth interplanetary coronal mass ejections during solar cycle 23 (1996–2009): Catalog and summary of properties. *Sol Phys* **264**: 189–237. DOI: 10.1007/s11207-010-9568-6.

Rouillard A, Lavraud B, Génot V, Bouchemit M, Dufourg N, et al. 2017. A propagation tool to connect remote-sensing observations with in-situ measurements of heliospheric structures. *Planet Space Sci* **147**: 61–77. DOI: 10.1016/j.pss.2017.07.001.

Vršnak B, Žic T, Vrbanec D, Temmer M, Rollett T, et al. 2013. Propagation of interplanetary coronal mass ejections: the drag-based model. *Sol Phys* **285**: 295–315. DOI: 10.1007/s11207-012-0035-4.

Winslow RM, Lugaz N, Philpott LC, Schwadron NA, Farrugia CJ, Anderson BJ, Smith CW. 2015. Interplanetary coronal mass ejections from MESSENGER orbital observations at Mercury. *J Geophys Res (Space Phys)* **120(8)**: 6101–6118. DOI: 10.1002/2015JA021200.

Winslow RM, Schwadron NA, Lugaz N, Guo J, Joyce CJ, et al. 2018. Opening a window on ICME-driven GCR modulation in the inner solar system. *ApJ* **856**: 139. DOI: 10.3847/1538-4357/aab098.

Witasse O, Sánchez-Cano B, Mays ML, Kajdič P, Opgenoorth H, et al. 2017. Interplanetary coronal mass ejection observed at STEREO-A, Mars, comet 67P/Churyumov-Gerasimenko, Saturn, and New Horizons en route to Pluto: Comparison of its Forbush decreases at 1.4, 3.1, and 9.9 AU. *J Geophys Res (Space Phys)* **122**: 7865–7890. DOI: 10.1002/2017JA023884.

**Cite this article as**: Grison B, Souček J, Krupar V, Píša D, Santolík O, et al. 2018. Shock deceleration in interplanetary coronal mass ejections (ICMEs) beyond Mercury's orbit until one AU. *J. Space Weather Space Clim.* **8**, A54.